Geochemical Journal, Vol. 47, pp. 185 to 199, 2013

Boron and other trace element constraints on the slab-derived component in Quaternary volcanic rocks from the Southern Volcanic Zone of the Andes

HIRONAO SHINJOE,[1]* YUJI ORIHASHI,[2] JOSÉ A. NARANJO,[3] DAIJI HIRATA,[4] TOSHIAKI HASENAKA,[5] TAKAAKI FUKUOKA,[6] TAKASHI SANO[7] and RYO ANMA[8]

[1]Tokyo Keizai University, Japan
[2]Earthquake Research Institute, The University of Tokyo, Japan
[3]Servicio Nacional de Geología y Minería, Chile
[4]Kanagawa Prefectural Museum of Natural History, Japan
[5]Department of Earth and Environmental Sciences, Graduate School of Science and Technology, Kumamoto University, Japan
[6]Department of Environment Systems, Faculty of Geo-environmental Science, Rissho University, Japan
[7]Department of Geology and Paleontology, National Museum of Nature and Science, Japan
[8]Integrative Environmental Sciences, Graduate School of Life and Environmental Sciences, Tsukuba University, Japan

(*Received April 18, 2012; Accepted December 25, 2012*)

We present a dataset for boron and other trace element contents obtained from samples from 13 volcanoes distributed along the Quaternary volcanic front of the Southern Volcanic Zone (SVZ) of the Chilean Andes. The dataset shows constraints on the nature of slab-derived component to mantle source. Analyzed samples show large negative Nb and Ta anomalies, and enrichment of alkaline earth elements and Pb, which are features of typical island arc volcanic rocks. Boron contents of SVZ volcanic rocks range 2.3–125.5 ppm, exhibiting marked enrichment relative to N-MORB and OIB. Both the boron contents and B/Nb ratios of the volcanic rocks increase from the southern SVZ (SSVZ) to central SVZ (CSVZ). Fluid mobile/immobile element ratios (B/Nb, Ba/Nb, Pb/Nb, and K/Nb) are used to examine slab-derived component to mantle source. Trace element compositions of altered oceanic crust (AOC)-derived fluid, sediment-derived fluid, and sediment melt are modeled. Mantle sources of volcanic rocks in CSVZ with high B/Nb ratios were contaminated by both AOC-derived and sediment-derived fluids. In contrast, mantle sources of volcanic rocks in SSVZ with a low B/Nb ratio were contaminated with *ca*. 3 wt% melt of subducted sediment, which had suffered from loss of boron during progressive devolatilization before melting.

Keywords: Andean Arc, arc lava, boron, prompt γ-ray analysis, mantle source

INTRODUCTION

The behavior of boron in arc volcanic rocks has received great attention because of its potential to trace the chemical flux to the mantle source of arc magma from the descending oceanic plate (Leeman and Sisson, 1996), because of the enrichment of boron both in altered oceanic crust (AOC) and sea floor sediment (Ishikawa and Nakamura, 1993; Smith *et al*., 1995), and because of its high fluid-mineral distribution coefficient during dehydration of the descending oceanic crust and sediment (Moran *et al*., 1992; Bebout *et al*., 1999). Boron abundance and ratios of boron to other trace elements with similar melt-mineral distribution coefficients but much lower fluid-mineral distribution coefficients (e.g., B/Be and B/Nb) have been applied widely for estimation of the contribution of slab-derived fluid to the mantle wedge. For example, boron abundance and its element ratios of arc volcanic rocks decrease from the volcanic front to the rear arc, which suggests that inventories of slab-derived boron in the mantle source decrease across the arc (Ryan *et al*., 1995; Ishikawa and Tera, 1997). Ratios of boron to fluid immobile elements have also been applied to determine whether AOC or the sediment cover of the slab is the dominant source of the fluid (Sano *et al*., 2001).

This paper presents new measurements of boron and other trace element concentrations in regional representative lavas obtained from 13 volcanoes on the Quaternary volcanic front of the Southern Volcanic Zone (SVZ) of the Andean arc in Chile. Boron abundances of volcanic rocks in the SVZ were reported previously as part of the studies of the contribution of slab-derived component to the magma source of volcanic rocks from circum-Pacific island arcs (Morris *et al*., 1990; Noll *et al*., 1996). This

*Corresponding author (e-mail: shinjoe@tku.ac.jp)

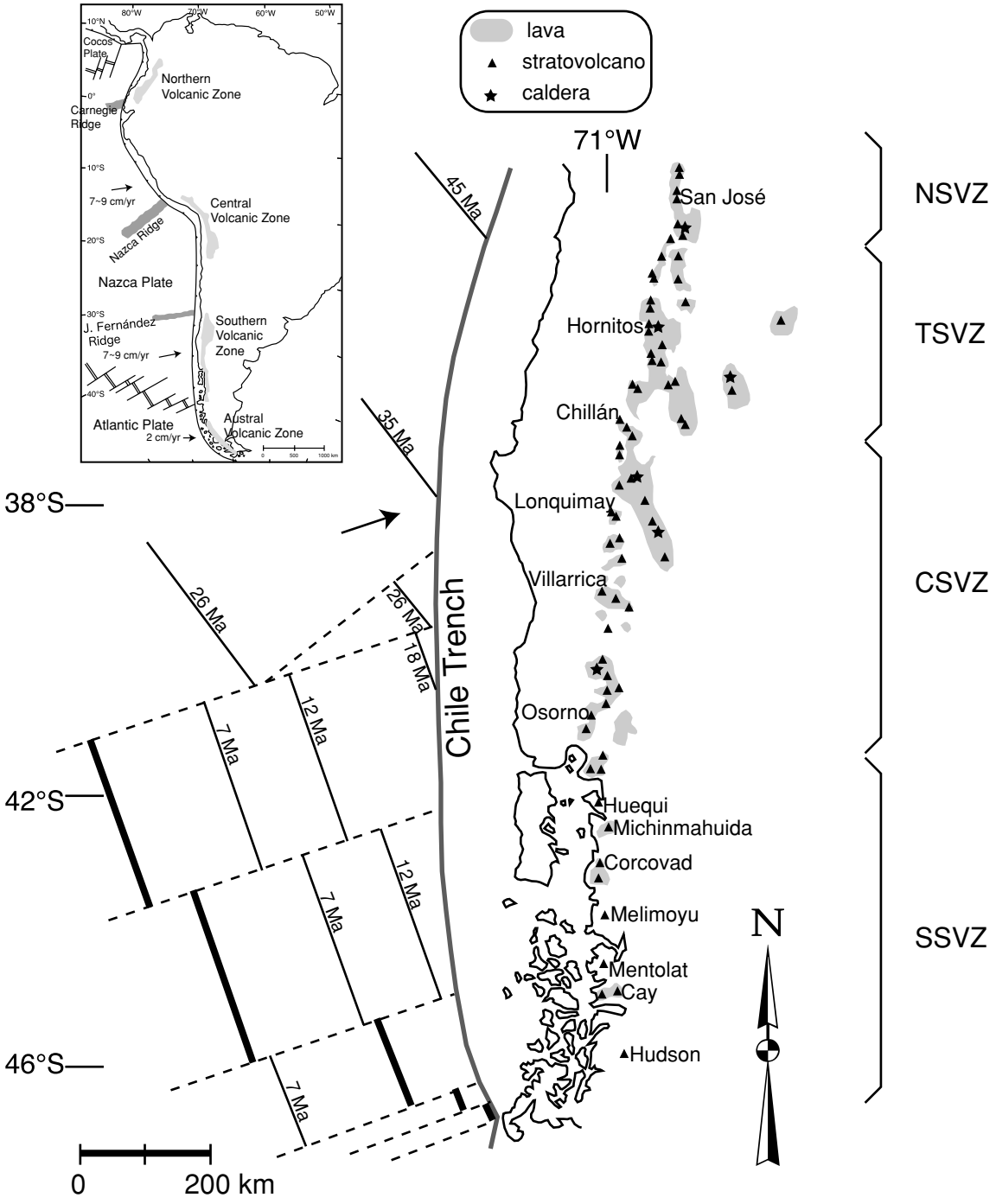

Fig. 1. Index map of the Southern Volcanic Zones (modified from Stern, 2004). Names of volcanoes where analyzed samples were obtained are also shown. The inset shows locations of the main map (box).

study was undertaken to present the overall along-arc variation of the ratios of fluid-mobile elements including boron to fluid-immobile elements for volcanic rocks on the volcanic front of SVZ, and to evaluate the contribution of the slab-derived component to the magma source of SVZ.

GEOLOGY

The Andean arc, which extends > *ca*. 7,500 km along the western margin of South America, is divided into four volcanic regions: the Northern (NVZ), Central (CVZ), Southern (SVZ), and Austral (AVZ) Volcanic Zones

(Stern, 2004; Fig. 1). The SVZ (33–46°S) is bordered by the Pampean volcanic gap corresponding to the subduction of the Juan Fernández Ridge to the north, and by the Patagonian volcanic gap marked by the Chile Triple Junction where the Chile Rise collides with the Taitao Peninsula to the east. The SVZ is a *ca*. 1400 km chain of more than 60 historically and potentially active volcanoes with numerous small eruptive centers (Stern, 2004; Stern *et al*., 2007). SVZ is subdivided into the northern (NSVZ, 33–34.5°S), transitional (TSVZ, 34.5–37°S), central (CSVZ, 37–41.5°S), and southern (SSVZ, 41.5–46°S) segments (Stern, 2004; Fig. 1) based on petrographical and geochemical features of volcanic rocks and tectonic considerations (Futa and Stern, 1988; Tormay *et al*., 1991; López-Escobar *et al*., 1993; Hickey-Vargas *et al*., 2002).

The SVZ is formed by subduction of the Nazca plate (0–45 Ma) beneath the South American plate at a rate of 7–9 cm/yr in a direction of 22–30° NE, orthogonal to the Chile trench. The subduction angle increases southward from *ca*. 20° to >25° (Stern, 2004). The thickness of the continental crust beneath the SVZ decreases southward. Crustal thickness of the NSVZ is inferred to be >55 km (Stern, 2004). In the TSVZ, crustal thickness inferred from gravity data decreases from 55 km at 34.5°S to 35 km at 37°S (Hildreth and Moorbath, 1988). For the CSVZ and SSVZ, south of 37°S, the crustal thickness is 30–35 km (Lowrie and Hey, 1981). General correlation between the continental crust thickness and the predominant volcanic rocks has been demonstrated. In the NSVZ, where the continental crust is thick, the predominant magmatic products are andesites and dacites. In contrast, in CSVZ and SSVZ, basalts and basaltic andesites are prominent products (López-Escobar *et al*., 1993).

Methods

Sampling sites

Samples analyzed in this study were obtained from 13 volcanoes of SVZ: San José, Hornitos, Chillán, Lonquimay, Villarrica, Osorno, Huequi, Michinmahuida, Corcovad, Melimoyu, Mentolat, Cay, and Hudson, from north to south (Fig. 1).

Two samples (012001aY and 012003aY) from the San José volcano in NSVZ are from upper Pleistocene lava flow on the western to northwestern skirt of the central crater of San José. Another two samples of San José (012005aY and 012103Y) were collected from upper Pleistocene to Holocene lava flows on the northern to western side of the central crater of San José (López-Escobar *et al*., 1985).

Two basaltic samples (011304Y and 011306Y) from the Hornitos volcano in TSVZ are from a small cone on the southwest flank of Cerro Azul (Gonzalez-Ferran, 1994). Chillán volcano is a volcanic cone of the Nevados de Chillán, a large composite stratovolcanic complex in TSVZ (Dixon *et al*., 1999). We obtained two samples (011501Y and 011505Y) of Holocene dacite lava flow (LT5; Dixon *et al*., 1999) from the Chillán volcano.

Six samples of Lonquimay volcano in CSVZ were obtained from lava flow from the central cone of the volcano. Two samples (LON-29, and 40) were collected from lava flow of the 1988–1990 eruption on the northeastern flank of the Lonquimay stratocone (Naranjo *et al*., 1992). We collected three samples (020506YA, 020602YA, and 020602YC) from Villarrica volcano in CSVZ. Sample 020506YA is from Pleistocene interglacial lava flow (Villarrica I; Hickey-Vargas *et al*., 1989) in the northern skirt of Villarrica volcano. Samples 020602YC (Villarrica II; Hickey-Vargas *et al*., 1989) and 020602YA (Villarrica III; Hickey-Vargas *et al*., 1989), which were collected at NNE foothill of the volcano, respectively derive from post-glacial lava flow and 1984-eruption lava flow. Two samples (OSO-11 and 35) were obtained from Osorno volcano, a Late Pleistocene to recent composite stratovolcano in CSVZ (López-Escobar *et al*., 1992). OSO-11 was collected from lava flow (Osorno3; López-Escobar *et al*., 1992) at the southern hillside of the summit. OSO-35 was taken from lava flow (Osorno2; López-Escobar *et al*., 1992) along the Rio Blanco in the northern skirt of Osorno volcano.

The samples from Huequi, Michinmahuida, Corcovad, Melimoyu, Mentolat, and Cay volcanoes in SSVZ (Heu-1, Mic-1, Cor-3, Mel-3, Men-3, and Cay-4, respectively) are the same as those from which López-Escobar *et al*. (1993) previously reported geochemical data with a brief petrographic description. Heu-1, Mic-1, and Cor-3 are andesite; the others are basalt in composition (López-Escobar *et al*., 1993). From Hudson, the southernmost volcano of SSVZ, three samples (HD1E1, HD1F1, and H4) were analyzed. HD1E1 and HD1F1 are basalt obtained from terminal moraine of outlet glacier on NNE flank of the edifice, and H4 is a basaltic andesite from pyroclastic flow deposit forming a lower part of the SE caldera (Orihashi *et al*., 2004). Petrographic descriptions and K–Ar ages of the Hudson samples were presented by Orihashi *et al*. (2004).

Geochemical analytics

Major and selected trace elements (Rb, Sr, Y, Zr, Zn, Ga, Co, Cr, Ni, V, and Sc) contents were determined using an X-ray fluorescence spectrometer (PW-2510; Philips Co.) at the Earthquake Research Institute, The University of Tokyo, using 1:2 dilution glass beads. Details of the analytical procedures were described by Tani *et al*. (2002). Other trace elements including rare earth elements (REEs) were analyzed using ICP-MS (VG Plasma Quad 3) with a frequency quintupled (λ = 213 nm) Nd-YAG laser ablation system (UP-213; New Wave Research Inc.)

Table 1. Whole rock chemical compositions of volcanic rocks in the Southern Volcanic Zone

Sample No.	012001AY	012003AY	012005AY	0121003Y	011304Y	011306Y	011501Y	011505Y	LON8	LON14	LON20	LON24	LON29	LON35	LON40
Location	San José	San José	San José	San José	Hornitos	Hornitos	Chillán	Chillán	Lonquimay	Lonquimay	Lonquimay	Lonquimay	Lonquimay	Lonquimay	Lonquimay
SiO_2 (wt%)	61.44	65.20	61.17	61.80	53.42	54.06	68.63	68.76	50.63	59.91	59.90	60.75	55.49	50.42	62.45
TiO_2	0.76	0.64	0.83	0.73	0.83	0.84	0.71	0.62	1.14	1.01	0.85	0.73	1.21	1.16	0.60
Al_2O_3	17.15	16.44	17.26	15.93	17.42	17.66	14.34	14.60	19.25	15.73	16.20	16.01	16.25	19.61	16.09
Fe_2O_3	5.99	4.57	5.67	5.60	8.18	8.26	4.39	4.16	10.07	8.89	8.86	8.45	9.67	10.33	7.92
MnO	0.10	0.09	0.09	0.10	0.14	0.14	0.09	0.09	0.17	0.21	0.23	0.23	0.22	0.18	0.23
MgO	2.48	1.76	2.33	3.04	5.18	5.28	0.75	0.85	3.91	1.50	1.29	1.04	2.08	3.96	0.74
CaO	5.12	3.20	5.13	4.90	9.42	9.52	2.20	2.40	9.88	4.57	4.53	4.21	5.60	9.72	3.77
Na_2O	4.01	4.53	4.16	3.92	3.28	3.31	5.02	4.95	3.37	5.34	5.52	5.61	5.13	3.33	5.82
K_2O	2.57	2.97	2.51	2.55	1.00	1.00	3.14	3.08	0.52	1.31	1.19	1.26	1.00	0.49	1.37
P_2O_5	0.19	0.22	0.20	0.19	0.17	0.18	0.16	0.13	0.18	0.39	0.35	0.28	0.46	0.17	0.21
Total	99.81	99.62	99.35	98.74	99.04	100.25	99.44	99.63	99.11	98.85	98.92	98.57	97.11	99.35	99.20
B (ppm)	28.3	19.3	25.4	14.1	14.4	13.3	114.0	126.0	21.3	58.7	47.1	49.4	41.8	13.8	49.3
Sc	12	8.8	12	14	30	30	12	12	33	23	25	23	26	33	26
V	117	89	115	111	235	240	27	32	248	29	12	6	40	280	6
Cr	6	6	3	44	77	78	n.d.	3	40	1	1	0	n.d.	41	2
Co	15	9	13	16	26	27	4	4	27	9	5	2	10	29	2
Ni	4	5	1	23	16	15	n.d.	1	11	n.d.	n.d.	n.d.	n.d.	11	n.d.
Zn	78	86	80	73	73	74	82	79	88	126	130	132	124	83	122
Ga	20	20	20	18	18	18	19	19	20	22	22	23	22	19	22
Rb	95	107	85	91	22	22	109	108	10	30	26	29	21	10	31
Sr	403	381	447	408	679	677	210	227	534	394	418	396	475	520	367
Y	28	21	26	22	15	16	38	35	25	56	54	56	38	21	59
Zr	182	232	177	173	84	83	325	295	125	311	325	340	123	70	378
Nb	11.3	14.1	11.4	11.5	1.9	1.9	9.5	8.8	1.5	3.8	3.5	3.6	3.0	1.3	3.6
Cs	2.3	2.9	2.5	1.7	1.3	1.4	6.1	7.3	1.1	2.8	2.4	2.4	1.9	0.5	2.6
Ba	432	634	430	460	249	249	612	603	175	407	390	423	338	181	379
La	28.1	34.1	28.5	30.0	11.3	10.9	31.5	28.0	7.4	19.7	18.0	19.0	16.1	7.4	18.4
Ce	54.1	65.5	56.7	56.0	21.8	21.7	62.2	59.7	16.8	42.1	38.9	39.4	33.8	16.1	39.2
Pr	6.5	7.4	6.5	6.6	3.0	3.0	8.1	7.2	2.5	6.1	5.6	5.8	5.1	2.4	5.7
Nd	26.8	28.3	26.8	26.0	14.3	13.8	35.6	30.3	12.2	30	27.7	28.2	26.1	12.8	27.9
Sm	5.41	5.21	5.76	5.24	3.14	3.18	8.05	6.80	3.32	8.22	6.93	7.24	6.74	3.42	7.66
Eu	1.27	1.23	1.22	1.18	1.10	1.11	1.63	1.43	1.25	2.48	2.34	2.42	2.26	1.27	2.31
Gd	4.87	4.68	4.68	4.28	2.71	2.56	7.26	5.75	2.95	7.42	6.47	6.75	6.24	3.14	6.91
Tb	0.73	0.65	0.69	0.60	0.44	0.41	1.12	0.94	0.50	1.25	1.19	1.21	1.08	0.57	1.16
Dy	4.28	3.25	3.97	3.71	2.41	2.42	6.79	5.78	3.16	7.80	6.65	7.23	6.38	3.45	7.26
Ho	0.93	0.69	0.85	0.75	0.54	0.50	1.40	1.21	0.71	1.61	1.50	1.57	1.31	0.71	1.50
Er	2.54	1.96	2.35	2.04	1.40	1.38	4.00	3.20	1.77	4.49	3.96	4.23	3.45	1.97	4.18
Tm	0.39	0.29	0.33	0.30	0.20	0.23	0.58	0.46	0.25	0.63	0.55	0.63	0.54	0.29	0.59
Yb	2.79	2.13	2.26	2.26	1.46	1.40	4.09	3.47	1.83	4.51	4.07	4.47	3.66	2.06	4.21
Lu	0.41	0.32	0.39	0.33	0.22	0.22	0.59	0.54	0.29	0.73	0.62	0.66	0.56	0.28	0.68
Hf	4.96	6.14	4.82	4.68	2.18	2.05	10.24	8.64	2.79	8.87	8.67	9.47	3.51	1.73	8.27
Ta	0.80	1.01	0.68	0.89	0.11	0.12	0.56	0.53	0.07	0.22	0.20	0.20	0.16	0.09	0.20
Pb	12.15	16.38	14.23	14.58	9.35	8.35	19.45	21.57	5.70	14.15	12.93	12.39	9.76	4.61	13.18
Th	11.34	11.62	11.08	12.58	3.34	3.36	12.24	12.69	1.42	4.51	3.38	4.01	3.94	1.97	4.20
U	3.02	4.05	2.71	3.51	0.79	0.78	2.66	3.11	0.36	1.07	0.95	0.95	0.79	0.35	1.00

Sample No.	LON50	020506YA	020602YA	020602YC	OSO11	OSO35	HUE-1	MIC-1	COR-3	MEL-2	MEN-3	CAY-4	HD4	HD1E1	HD1F1
Location	Lonquimay	Villarica	Villarica	Villarica	Osorno	Osorno	Huequi	Michinmahuida	Corcovado	Melimoyu	Mentolat	Cay	Hudson	Hudson	Hudson
SiO_2 (wt%)	54.32	52.85	52.33	52.70	51.55	58.13	58.48	51.26	51.68	53.55	54.33	51.79	54.04	52.43	52.77
TiO_2	1.51	1.24	1.29	1.36	0.81	1.02	0.63	1.05	1.00	1.60	1.08	1.75	1.39	2.24	1.36
Al_2O_3	16.25	16.35	16.18	16.80	20.42	17.68	18.11	20.38	18.15	17.85	18.08	16.22	16.80	15.66	17.27
Fe_2O_3	11.31	10.02	10.30	10.39	8.35	8.33	7.01	8.61	8.91	9.48	9.01	11.40	9.16	10.80	9.36
MnO	0.21	0.16	0.16	0.16	0.14	0.16	0.14	0.12	0.15	0.16	0.17	0.19	0.16	0.19	0.16
MgO	3.04	4.89	6.09	5.07	4.64	2.95	2.94	3.96	5.50	3.09	3.52	4.30	4.23	4.02	4.94
CaO	6.66	9.42	9.31	9.58	10.85	6.86	6.73	10.78	9.92	7.58	7.98	8.59	8.35	7.87	9.38
Na_2O	4.48	3.26	3.09	3.24	2.80	4.11	3.67	3.13	2.96	4.17	3.79	3.25	4.06	4.50	3.77
K_2O	0.87	0.72	0.68	0.80	0.46	0.86	0.76	0.63	0.61	1.46	0.55	1.27	1.21	1.30	1.01
P_2O_5	0.32	0.72	0.68	0.80	0.46	0.86	0.76	0.63	0.61	0.42	0.25	0.47	0.52	0.84	0.33
Total	98.97	99.15	99.68	100.38	100.13	100.30	98.69	100.12	99.06	99.36	98.76	99.21	99.92	99.86	100.36
B (ppm)	38.1	24.6	32.2	33.5	11.6	13.4	19.4	2.9	6.0	12.6	7.2	16.5	5.2	2.3	4.4
Sc	31	36	34	35	30	24	14	28	30	28	25	34	29	30	33
V	178	295	286	315	231	172	87	246	222	255	207	292	223	265	250
Cr	n.d.	86	148	102	81	4	3	65	78	n.d.	10	41	42	9	57
Co	22	28	33	32	26	16	14	25	30	20	20	30	23	23	26
Ni	n.d.	29	64	48	25	1	2	28	28	4	5	25	16	10	16
Zn	108	90	89	94	73	97	78	81	76	96	95	109	88	97	81
Ga	18	18	17	19	17	18	17	19	17	19	19	18	17	18	18
Rb	20	17	16	19	13	24	18	8.6	14	35	12	34	28	21	21
Sr	466	435	437	443	404	362	407	610	414	490	439	369	591	573	701
Y	45	26	25	29	17	30	19	19	21	32	30	43	31	40	26
Zr	278	97	97	114	60	176	118	93	92	179	111	206	200	204	141
Nb	2.6	2.2	2.0	2.7	1.5	3.8	5.1	2.4	3.6	12.5	3.8	9.9	9.0	12.5	6.4
Cs	1.8	1.4	1.4	1.6	0.8	0.6	1.2	0.2	0.5	1.4	1.4	1.4	0.7	1.2	0.8
Ba	283	205	200	226	123	238	253	184	199	403	184	313	418	444	316
La	13.3	9.8	9.0	11.4	5.7	11.7	13.4	10.4	12.0	29.9	10.3	24.6	29.9	38.5	21.7
Ce	28.6	19.8	19.1	23.4	12.0	24.2	27.1	20.9	23.3	52.1	22.8	48.8	58.2	73.0	42.0
Pr	4.3	3.1	3.0	3.5	1.7	3.3	3.7	2.9	3.2	7.0	3.5	7.1	7.7	9.9	5.6
Nd	21.2	15.4	15.1	17.6	8.9	15.7	16.5	14.6	14.7	30.8	17.4	34.1	33.8	44.7	25.7
Sm	5.73	4.16	4.17	4.73	2.46	4.05	3.67	3.51	3.55	6.82	4.67	8.25	7.18	9.17	5.42
Eu	1.90	1.30	1.31	1.45	0.91	1.41	1.21	1.29	1.23	2.04	1.52	2.17	2.19	3.02	1.84
Gd	5.15	3.93	4.04	4.25	2.37	3.70	3.07	3.25	3.38	6.28	4.13	7.59	6.46	8.43	4.88
Tb	0.92	0.71	0.68	0.78	0.43	0.70	0.50	0.55	0.55	1.01	0.79	1.32	0.96	1.23	0.70
Dy	5.62	4.38	4.27	4.74	2.73	4.13	3.04	3.20	3.49	5.66	4.59	7.61	5.46	7.22	4.46
Ho	1.19	0.93	0.94	0.97	0.59	0.89	0.63	0.65	0.76	1.17	0.98	1.56	1.07	1.47	0.89
Er	3.05	2.54	2.54	2.73	1.61	2.54	1.77	1.75	2.05	3.28	2.64	4.38	3.04	3.88	2.43
Tm	0.49	0.36	0.37	0.41	0.23	0.37	0.26	0.24	0.31	0.45	0.40	0.64	0.43	0.54	0.35
Yb	3.31	2.51	2.64	2.83	1.54	2.60	1.79	1.83	2.02	3.19	2.79	4.31	3.04	3.64	2.29
Lu	0.49	0.39	0.36	0.43	0.23	0.40	0.33	0.26	0.31	0.47	0.41	0.67	0.46	0.52	0.35
Hf	7.51	2.58	2.68	3.11	1.65	4.30	2.95	2.15	2.20	4.72	2.73	5.29	4.75	4.92	3.25
Ta	0.14	0.11	0.12	0.14	0.09	0.21	0.27	0.12	0.20	0.68	0.18	0.52	0.43	0.71	0.35
Pb	9.38	5.80	5.59	6.91	3.96	6.12	3.94	3.05	3.73	7.56	4.19	7.30	6.03	6.20	5.30
Th	3.58	1.59	1.36	1.90	1.10	2.81	2.77	1.79	2.31	7.21	1.79	4.30	4.32	7.75	5.92
U	0.67	0.41	0.41	0.48	0.27	0.51	0.42	0.44	0.44	1.21	0.26	0.88	0.74	1.16	0.73

at the Earthquake Research Institute, The University of Tokyo. Glass beads used for the XRF analysis also appropriated for laser ablation ICP-MS analysis. Element abundances were corrected internally using Sr concentrations determined from XRF analysis. Details of the analytical procedures followed those of Orihashi and Hirata (2003).

Boron contents were determined using prompt γ-ray analysis (PGA) at the thermal neutron beam guide of the JRR-3M reactor, Japan Atomic Energy Agency (Yonezawa, 1993). Powdered samples were dried for 24 h at 110°C. Disks (12 mm diameter, 2–3 mm thickness) containing about 0.7 g of the samples were created by cold pressing. The disks were heat-sealed in 25 mm-thick fluorinated ethylene propylene resin film. A Compton suppression PGA spectrum was accumulated for 1000–7000 s. Standards of the Geological Society of Japan JB-1a and JB-2 were used for calibrating the B content determination. The count rate was corrected by Si factor (Si count rate divided by SiO_2 content of the sample) to exclude effects from the fluctuation of neutron flux and from the variation of sample geometry. Details of the analytical procedures were described by Sano *et al*. (1999).

RESULTS

Overall major and trace element characteristics

Major and trace element compositions of volcanic rocks in SVZ obtained in this study are presented in Table 1. Most analyzed samples are medium-K basalt, basaltic andesite, andesite, and dacite in the K_2O–SiO_2 diagram (Fig. 2). Two andesites from SSVZ (Huequi and Mentolat) are within the low-K field, and samples from San José and Chillán are high-K andesite and dacite. N-MORB normalized incompatible element patterns are depicted in Fig. 3. All of the SVZ volcanic rocks have negative Nb and Ta anomalies, general enrichments of the highly incompatible elements, and pronounced positive Pb concentration "spikes". All are features that are typically observed island arc volcanic rocks.

Boron contents of most SVZ volcanic rocks are 2.3–58.7 ppm, which is within the range of the boron concentrations of circum-Pacific island arc volcanic rocks (e.g., Morris *et al*., 1990), and which shows marked enrichment relative to N-MORB and OIB (0.5 ppm and 1.1 ppm, respectively; Chaussidon and Marty, 1995). Two dacites from Chillán volcano are highly enriched in boron (114.3 and 125.5 ppm).

Along-arc variations of boron and other predominately slab-derived trace elements

Enrichment of boron in island arc volcanic rocks has been interpreted as reflecting the addition of slab-derived component to the magma source (Morris *et al*., 1990).

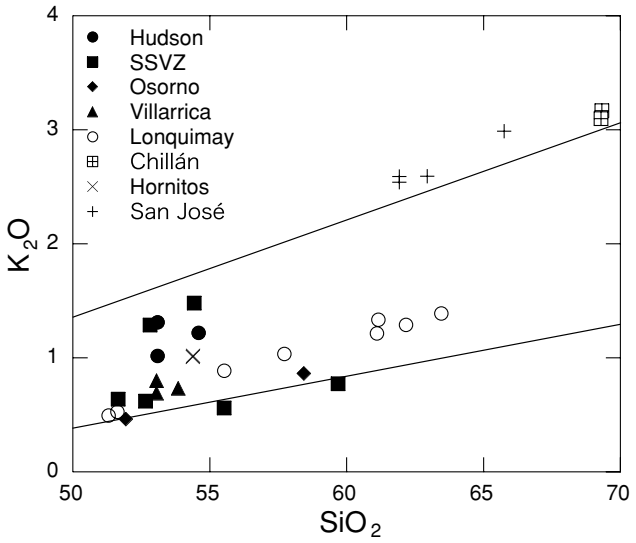

Fig. 2. K_2O versus SiO_2 (wt%) diagram of the analyzed samples.

Across-arc variation of boron contents has also been reported. High boron abundance in volcanic front lavas decreases across the arc (Ryan *et al*., 1995; Ishikawa and Tera, 1997; Miyoshi *et al*., 2008). The continuous depletion of boron reflects the gradual depletion of volatiles and fluid-mobile elements during dehydration of the subducting slab (Ishikawa and Tera, 1997). Our samples were obtained from the Quaternary volcanic front of SVZ. Therefore, we discuss the overall along-arc variation of boron and other incompatible elements.

In Fig. 4, boron contents show a relation to latitude. In general, andesites and dacites are more enriched in boron than in either basalts or basaltic andesites. This fact implies that boron enrichment occurs during fractional crystallization process because boron is incompatible with main crystal phases in basaltic and andesitic magmas (e.g., olivine, plagioclase, pyroxene). Basalts and basaltic andesites in SSVZ are more depleted in boron than those in CSVZ and TSVZ.

Boron and other fluid mobile elements' abundance patterns strongly reflect slab-derived fluid inputs. However, they are affected by varying degrees of partial melting and crystal fractionation. To disentangle these effects, we determine the ratios of boron and other fluid-mobile elements to other elements with similar solid-melt distribution coefficients (*Ds*) but much lower apparent solid-fluid *Ds*. Use of these element ratios can minimize the effects of processes (e.g., degree of partial melting and intra-crustal fractional crystallization) other than subduction modification of the mantle. In addition to boron, we adopt lead as a fluid-mobile element because a positive Pb concentration spike is prominent in N-MORB normal-

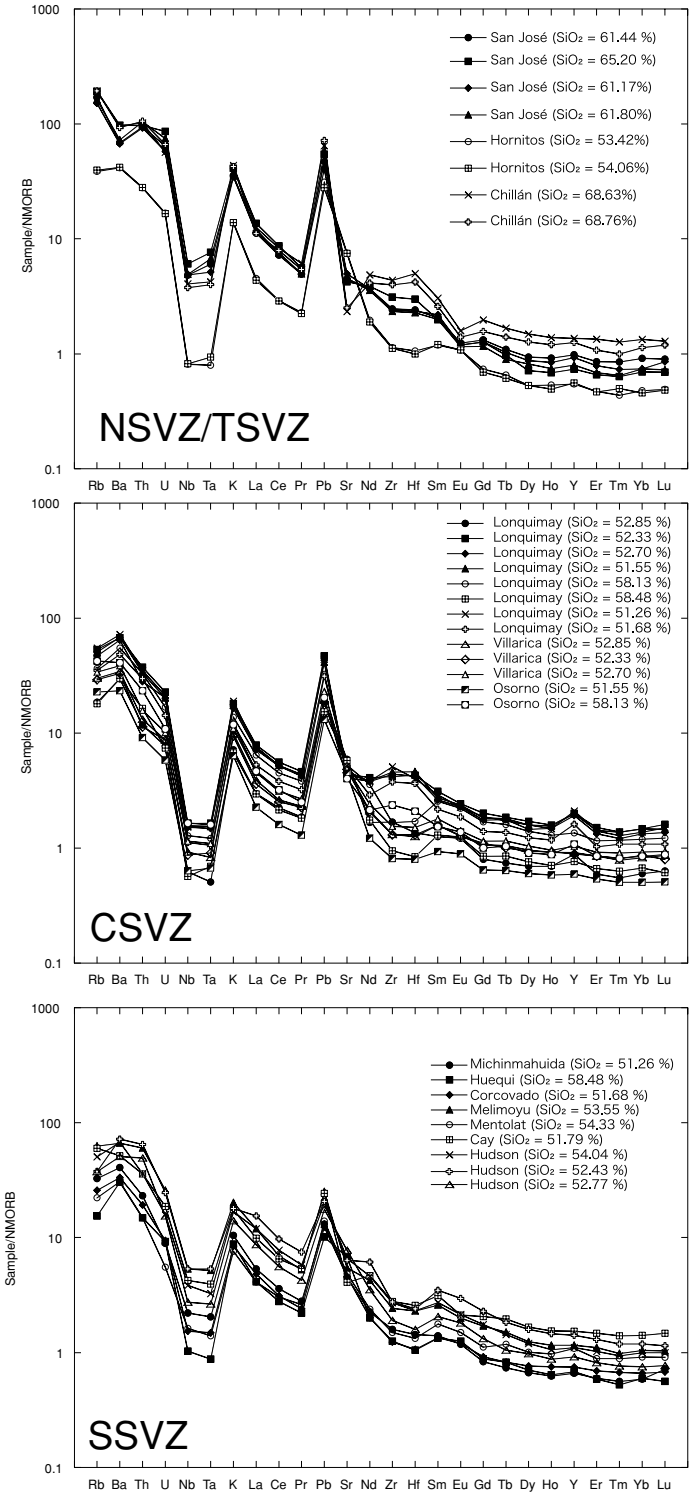

Fig. 3. N-MORB normalized incompatible element patterns of the SVZ volcanic rocks. a) northern and transitional SVZ, b) central SVZ, and c) southern SVZ. Normalized values are referred from Sun and McDonough (1989).

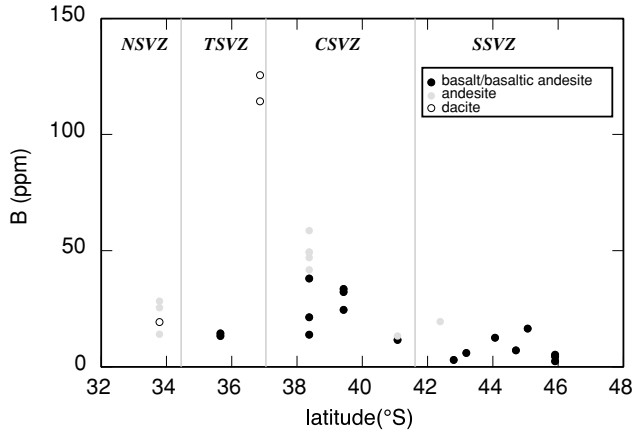

Fig. 4. Plots of boron concentrations of volcanic rocks in SVZ for the along-arc transect.

ized incompatible element patterns (Fig. 3). In addition, Ba and K are adopted as fluid-mobile elements because enrichment of these elements is observed for most samples (Fig. 3). We chose Nb and Zr as elements with similar solid-melt *Ds* but with much lower mobility than B, Ba, K, or Pb. Accordingly, in Fig. 5, B/Nb, Ba/Nb, K/Nb, Pb/Nb, B/Zr, Ba/Zr, K/Zr, and Pb/Zr ratios are shown versus latitudes. Element ratios of N-MORB are also shown for comparison (Sun and McDonough, 1989; Chaussidon and Marty, 1995). Analyzed samples of CSVZ include andesites, although it is notable that the ranges of these element ratios of andesites accord well with those of basalt/basaltic andesite.

The element ratios are higher than those of N-MORB. However, B/Nb and B/Zr ratios of Hudson volcano samples in SSVZ are comparable to those of N-MORB. Element ratios of basalts and basaltic andesites in SSVZ are uniformly lower than those of CSVZ and TSVZ, except for Ba/Zr and K/Zr: the addition of fluid-mobile elements to the mantle wedge was greater for CSVZ and TSVZ than for SSVZ. The dissimilar patterns of Ba/Zr and K/Zr might be ascribed to the greater difference of incompatibility of Ba and K from Zr than from Nb during the melting and crystal fractionation (Hoffman, 1988). Andesite and dacite samples from San José volcano in NSVZ show lower element ratios than those for basalts and basaltic andesites in CSVZ and TSVZ.

DISCUSSION

Estimation of trace element contents of slab-derived fluid

To evaluate the contribution of slab-derived fluid to the magma source of SVZ, trace element contents in the fluid from subducting sediments and AOC were estimated using the method described by Sano *et al*. (2001). Modelling was conducted for B, Ba, Pb, K, and Nb because element ratios of B/Nb, Ba/Nb, Pb/Nb, and K/Nb clearly reflect along-arc variation from SSVZ to CSVZ (Fig. 5). Element contents of the fluid were obtained using the following formula: (bulk composition of sediment or AOC) × (mobility of the element)/(weight fraction of fluid). Mobility of elements during the dehydration experiments is expressed as shown below.

$$Mobility = \frac{C_{STM} - C_{RP}}{C_{STM}}.$$

Therein, C_{STM} and C_{RP} respectively represent the concentration of an element in the starting material and in the run products (Kogiso *et al*., 1997). Mobility data used in this model were obtained from the results of high-pressure experiments for pelitic schists of high P/T metamorphic belt (Aizawa *et al*., 1999) and amphibolite (Kogiso *et al*., 1997). The trace element composition of the average of ODP Leg 144 sediment (Kilian and Behrmann, 2003) was adopted to represent the composition of subducted sediments, except for boron. The ODP Leg 144 sediment samples were obtained from the sites drilled into the accretionary prism and its cover sediment on the Nazca plate north of the Chile Triple Junction (Behrmann *et al*., 1994). For the boron contents of the sediments, averages of eight sediment samples from the sea floor near Chile Rise obtained by the Mirai MR08-06 cruise (see Supplementary Materials for details) were used. Trace element compositions of AOC were reported by Sano *et al*. (2001) and Kelley *et al*. (2003). Boron contents of AOC were obtained from data compiled by Smith *et al*. (1995). Weight fractions of fluid from subducted sediment and AOC were assumed to be 1.5 wt% (Kogiso *et al*., 1997). The parameters used and results of the calculations are presented in Table 2.

A B/Nb vs. K/Nb plot with model calculation of bulk mixing among the depleted mantle, the sediment-derived fluid, and the AOC-derived fluid is shown in Fig. 6. In spite of low B/Nb ratios, SSVZ samples show clearly higher K/Nb than those of depleted mantle. The high K/Nb ratio of SSVZ volcanic rocks cannot be explained by addition of slab-derived fluid to the depleted mantle. The same results were obtained for B/Nb vs. Ba/Nb, and B/Nb vs. Pb/Nb plots, which suggests that the mantle source of SSVZ volcanic rocks was metasomatized with higher K/Nb, Ba/Nb, and Pb/Nb ratios than those of depleted mantle.

The CSVZ samples are on the high B/Nb region, showing overall positive correlation between B/Nb and K/Nb ratios, which shows agreement with the trend formed by addition of slab-derived fluid to the magma source. Most CSVZ samples are of the K/Nb region higher than the

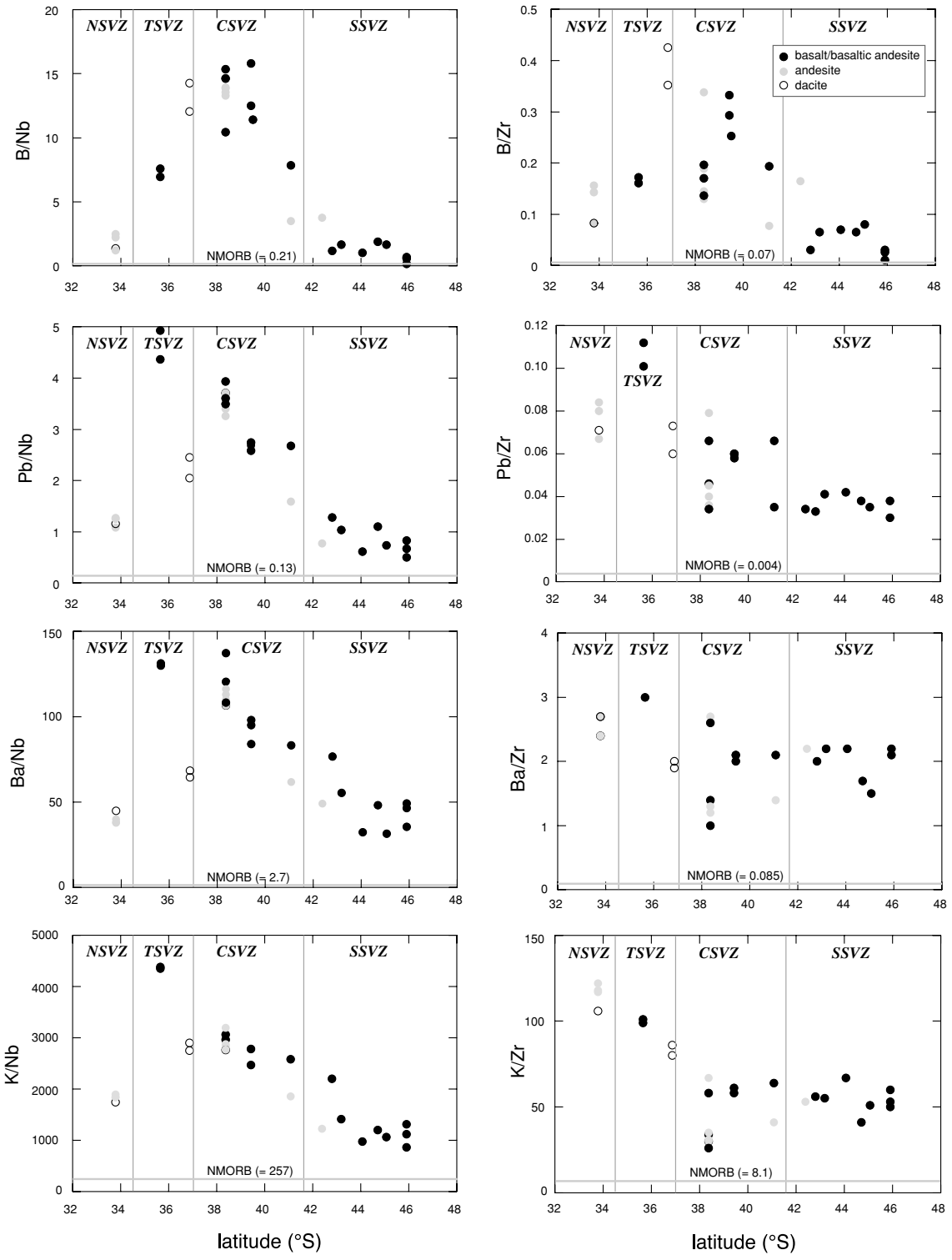

Fig. 5. Plots of fluid-mobile/immobile element ratios of the volcanic rocks in SVZ for the along-arc transect. NMORB values of ratios (Sun and McDonough, 1989; Chaussidon and Marty, 1995) are also shown for comparison.

Table 2. Model calculation of slab-derived fluid compositions in ppm

	Nb	B	Ba	Pb	K
AOC[a]	2.89	5.2	100	0.44	1250
Sediment[b]	9.1	58	445	13.3	17931
Depleted mantle[c]	0.1485	0.05	0.563	0.018	20
Mobilty (AOC)[d]	0.036	0.6	0.525	0.846	0.5
Mobility (sediment)[e]	0.021	0.7	0.076	0.65	0.12
AOC-derived fluid	6.9	208	3500	25	41667
Sediment-derived fluid	12.7	2707	2255	576	143448

[a]*Contents of AOC (altered oceanic crust) are from Sano et al. (2001) and Kelley et al. (2003).*
[b]*Contents of sediment are from Kilian and Behrmann (2003). For boron content of sediment, see Supplementary Materials.*
[c]*Contents of depleted mantle are from Wokrman and Hart (2005). Boron content of depleted mantle is taken from Chaussidon and Marty (1995).*
[d]*Mobilities of AOC are from Kogiso et al. (1997).*
[e]*Mobilities of sediment are from Aizawa et al. (1999).*

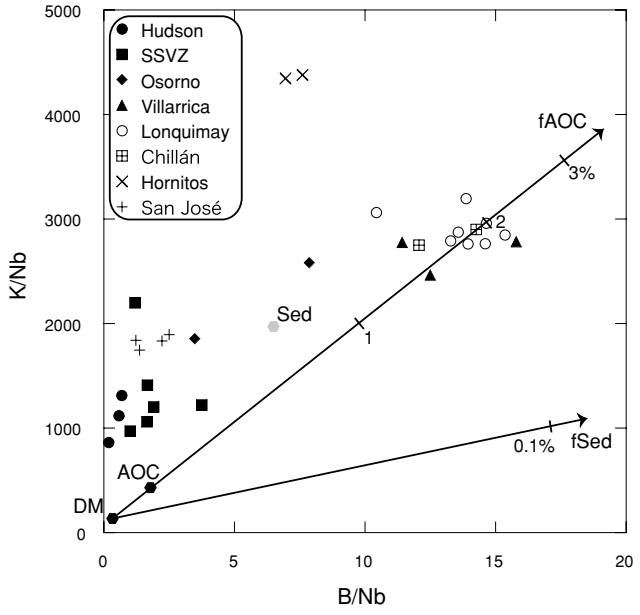

Fig. 6. Plots of B/Nb versus K/Nb of volcanic rocks in SVZ. Model calculations of mixing among the depleted mantle (DM), sediment-derived fluid, and AOC-derived fluid are also demonstrated. Compositions of the depleted mantle are from Workman and Hart (2005) and Chaussidon and Marty (1995). Compositions of sediments are from Kilian and Behrmann (2003). For boron concentrations of sediments, see Supplementary Materials.

mixing line between depleted mantle and slab-derived fluids. Therefore, sub-arc mantle before addition of slab-derived fluids shows a higher K/Nb ratio than those of depleted mantle.

Inferring the magma source of CSVZ rocks

Previous geochemical studies of the CSVZ basalts and basaltic andesites (e.g., Futa and Stern, 1988; Gerlach *et al*., 1988; Hickey-Vargas *et al*., 1989) have shown that CSVZ basalts originated from melting of mantle wedge peridotite metasomatized by fluid from the subducted slab including sediment. This inference of origin is supported by the high B/Nb ratios of CSVZ rocks based on our fluid model. However, most CSVZ samples are also of a K/Nb region higher than the mixing line between depleted mantle and slab-derived fluids (Fig. 6). In this section, candidates for sub-arc mantle with a higher K/Nb ratio than those of depleted mantle are examined.

Hickey-Vargas *et al*. (2002) reported that basalts from small eruptive centers (SECs) near the Villarrica volcano in CSVZ are poorer in fluid mobile elements than nearby Villarrica volcano basalts. Depletion of particularly fluid mobile elements is readily apparent. The range of B/Nb ratios is limited to low values (0.41–4.86). Furthermore, ranges of Ba/Nb, Pb/Nb, and K/Nb ratios largely overlap those of CSVZ volcanic rocks. In addition, SEC basalts have small $^{10}Be/^{9}Be$ ratios and near unity ($^{238}U/^{230}Th$) activity, which indicates that these rocks are from subduction material stored in the mantle wedge for 0.35 to 3 m.y. In contrast, composite center basalts of Villarrica volcano with high $^{10}Be/^{9}Be$ ratios were derived from mantle sources rich in fluid mobile elements that had been transferred recently from the subducted slab (Hickey-Vargas *et al*., 2002).

We therefore presumed the mantle composition estimated from the SEC basalts near Villarrica as equal to that of the mantle source of CSVZ before addition of slab-derived fluids. The composition of basalt with the lowest B/Nb ratio is used to infer B, Nb, Ba, Pb, and K concentrations of the magma source in the mantle wedge assuming 15% batch melting of lherzolite mantle source (olivine 50%, orthopyroxene 30%, clinipyroxene 20%). Partition coefficients between the melt and minerals are referred from Ottolini *et al*. (2009) for boron, and from Tatsumi (2000) for other elements.

In Fig. 7, mixing lines between the presumed CSVZ

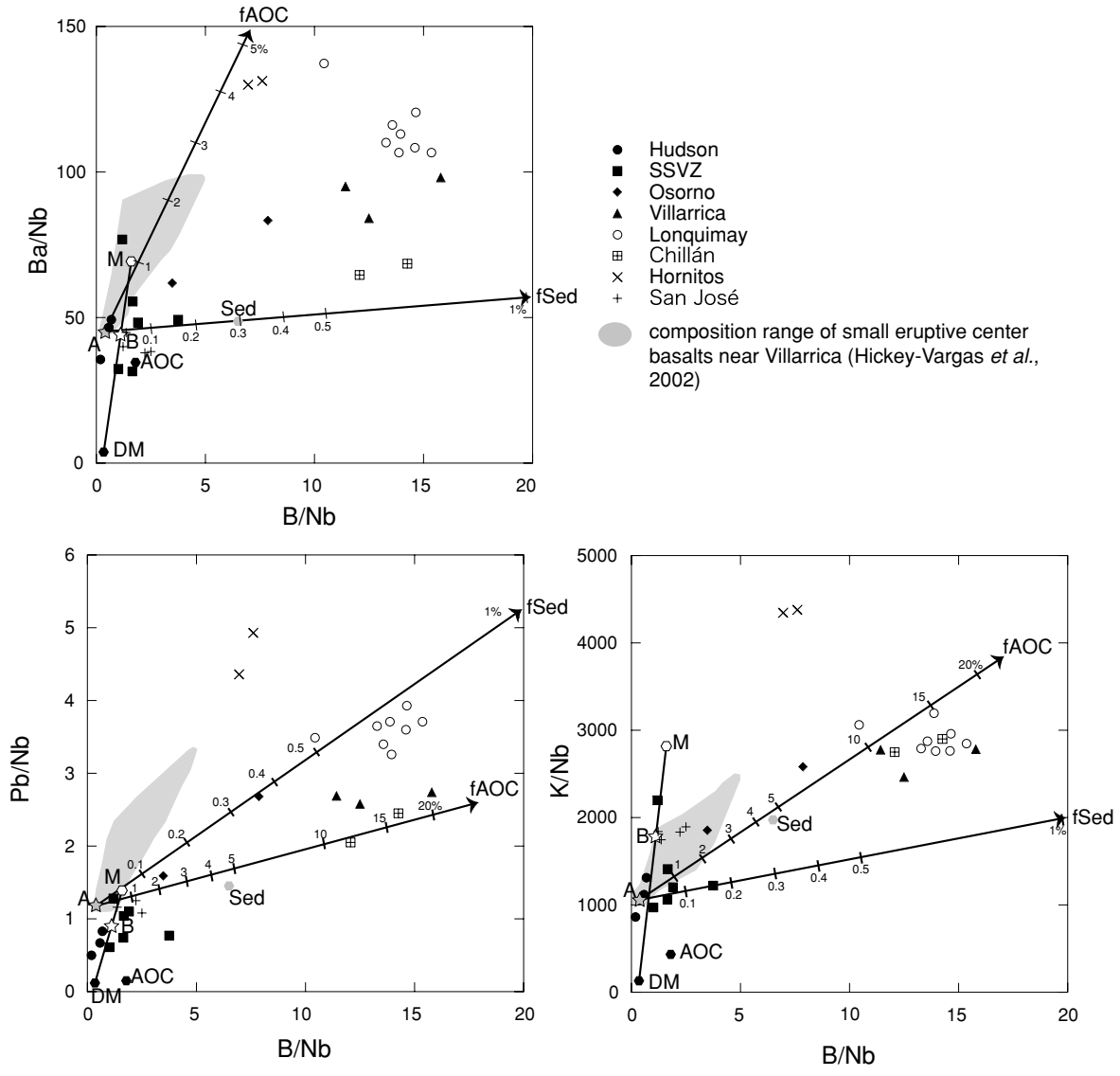

Fig. 7. Plots of B/Nb versus Ba/Nb, Pb/Nb, and K/Nb of volcanic rocks in SVZ. Hatched areas show ranges of basalts from small eruptive centers near Villarrica volcano in CSVZ (Hickey-Vargas et al., 2002). A: presumed sub-arc mantle beneath CSVZ before the addition of slab-derived fluids. Model calculations of bulk mixing among the presumed sub-arc mantle, sediment-derived fluid (fSed), and AOC-derived fluid (fAOC) are shown. Compositions of sediment-derived fluid and AOC-derived fluid are presented in Table 2. To show the mantle source of the SSVZ, model calculations of mixing between sediment melt (M) and depleted mantle (DM) are also shown. Compositions of sediment melt were calculated based on the solid-melt bulk distribution coefficients and the degree of melting obtained from high-pressure experiments (Johnson and Plank, 1999), and sediment composition from Kilian and Behrmann (2003). For estimation of the B/Nb ratio, see the text in detail. Point B corresponds to 3% bulk mixing of the calculated sediment melt to the depleted mantle.

mantle source before addition of slab-derived fluids (point A) and calculated fluids are demonstrated for B/Nb vs. Ba/Nb, Pb/Nb, and K/Nb. Composition ranges of SECs basalts near Villarrica volcano (Hickey-Vargas *et al*., 2002) are also demonstrated. Plots of samples from Osorno, Villarrica, and Lonquimay volcanoes show considerable scattering, although their B/Nb, Ba/Nb, Pb/Nb, and K/Nb ratios are explained by the addition of both AOC-derived and sediment-derived fluids to the presumed CSVZ mantle source. The amount of sediment-derived fluid is estimated as less than 1 wt%. The amount of AOC-derived fluid is estimated as less than 5 wt% based on the B/Nb vs. Ba/Nb model. However, larger amounts of AOC-derived fluid are necessary to explain K/Nb and Pb/Nb

ratios. This inconsistency might be ascribed to the large uncertainty in AOC composition (e.g., Smith *et al*., 1995; Kogiso *et al*., 1997). Additionally, SEC basalts used for inferring the CSVZ mantle source before addition of slab-derived fluids can cause considerable variation in K/Nb and Pb/Nb ratio (Fig. 7). Another uncertainty is the trench sediment composition. We used the trace element composition of sediment close to the Chile triple junction for the model calculation. However, to the north of 40°S, the late Paleozoic Coastal Batholith might provide trench sediment with distinct composition (Hervé *et al*., 2007).

For TSVZ volcanic rocks, dacites of the Chillán volcano are shown close to Lonquimay and Villarrica samples. Following our fluid addition model, the mantle source of Chillán volcano rocks was also metasomatized by slab-derived fluid, although it remains unclear whether felsic (SiO_2 = *ca*. 69 wt%) Chillán samples retain incompatible element ratios of primitive magma. Samples from Hornitos volcano with high Pb/Nb and K/Nb ratios, despite their moderately low B/Nb ratios, are inconsistent with our fluid model.

It is notable that samples from San José volcano in NSVZ are also shown in the low B/Nb region close to SSVZ samples. The continental crust thickness in NSVZ is inferred as >55 km. Therefore, effects of crustal contamination on the magma are believed to be considerable (López-Escobar *et al*., 1985). Moreover, our samples from San José are andesites and dacites with SiO_2 > 60%. Therefore, the effect of crystal fractionation on element ratios is greater than for more primitive lavas. Nevertheless, the $^{10}Be/^{9}Be$ ratios of sample from Villarrica and Osorno volcanoes are much higher than those from San José (Sigmarsson *et al*., 1990). Our data are consistent with the generally recognized correlation between $^{10}Be/^{9}Be$ and $B/^{9}Be$ for many island arc lavas including SVZ (Morris *et al*., 1990). These facts suggest that the contribution from recent dehydration of subducted sediment has been small for the San José mantle source. Alternatively, the material subducted below this region of the arc differs, including more terrigenous sediments (as in the SSVZ) or continental crust eroded tectonically from the continental margin by the subduction of the Juan Fernandez Ridge (Stern, 2004).

Hickey-Vargas *et al*. (2002) described two alternatives for the origin of the "older" mantle source of the small eruptive centers basalts, which is poor in fluid-mobile elements. One hypothesis is that the subduction component depleted in fluid-mobile elements was formed under hotter conditions than those which prevail now. However, reconstruction of the tectonic development of southern South America reveals that the Chile Triple Junction has moved northward at least during the last 10 Ma (e.g., Ramos and Kay, 1992). Therefore, the subducting Nasca plate beneath the CSVZ has become younger (= hotter) during this period. The other hypothesis is that fluid-mobile elements in water were expelled during the solidification process in the mantle wedge. A low B/Nb ratio despite the high Ba/Nb, Pb/Nb, and K/Nb ratios of Hornitos basalts (Fig. 7) might be explained by boron loss from the mantle source, which was suffered previously from addition of slab-derived fluid during similar processes such as those of the mantle source of small eruptive center basalts.

Estimation of the magma source of SSVZ rocks

Contamination of the slab derived component to the SSVZ mantle source has been discussed by D'Orazio *et al*. (2003) based on geochemical data of Cay and Maca volcanoes. They suggested that addition of small amounts (<1%) of both bulk sediment and slab-derived fluid to the depleted mantle is attributable to the mantle source of the Cay and Maca volcanoes. However, Kilian and Behrmann (2003) ruled out the slab-derived fluid as a possible contaminant of the mantle source because of the moderately low U/Th ratio of basalt in SSVZ. They also estimated that the mantle source of SSVZ basalt was contaminated by 3–5% of terrigenous sediment melt based on the mixing calculation of Pb–Sr–Nd isotopes. The low B/Nb ratios of SSVZ samples cannot reflect contamination by slab fluids. Therefore, the plausible slab-derived contamination agency is sediment melt, as suggested by Kilian and Behrmann (2003).

Assuming batch melting, the K, Ba, Pb, and Nb contents of sediment melt were calculated to estimate the mantle source composition of SSVZ. For sediment composition, we also adopted the average of ODP Leg 144 sediment (Kilian and Behrmann, 2003). Solid-melt bulk distribution coefficients (*Ds*) and the degree of melting (=0.26) were referred from results of high-pressure experiments reported by Johnson and Plank (1999). The K/Nb, Ba/Nb, and Pb/Nb ratios of the mantle source obtained by 3% addition of calculated melt to depleted mantle, as estimated by Kilian and Behrmann (2003), are well within the range of SSVZ basalts and basaltic andesites.

The bulk distribution coefficient of boron during the melting of sediment remains uncertain, but boron behaves as a moderately incompatible element in silicic rocks (Leeman and Sisson, 1996). Assuming that the *Ds* of boron is similar to that of niobium, then the B/Nb ratio of sediment melt, which is close to those of bulk sediment (=6.37), would considerably raise the B/Nb ratio of the mantle source. To explain the low B/Nb ratio of the SSVZ volcanic rocks, a lower B/Nb ratio is needed for the melt composition of the sediment on the subducting slab. One process to explain the low B/Nb is removal of boron by subtraction of H_2O-rich fluids from subducting sediments during progressive devolatilization. The concentrations, particularly of fluid mobile elements such as B, Cs, As,

and Sb in arc lavas from warmer subduction zones, are lower than those from cooler subduction zones (Bebout *et al*., 1999; Morris and Ryan, 2003). Indeed, in subduction zones where the prograde metamorphic *P–T* path passes through epidote-blueschist facies or higher T/P facies, considerable loss of B and Cs from subducting sediments is expected at depths shallower than *ca*. 45 km (Bebout, 2007). The degree of removal of boron in the forearc is uncertain. Therefore, we simply assumed that B/Nb ratio of the mantle source with 3% addition of sediment melt to depleted mantle equals the average B/Nb ratio of eight basalt/basaltic andesites of SSVZ (=1.11). In this case, the calculated B/Nb ratio of the sediment melt is 1.63. Assuming that the *Ds* of boron is equal to that of niobium, the boron concentration of sediment before melting is calculated as 14 ppm. This boron concentration is comparable to those of sediments that have undergone a loss of boron during subduction zone metamorphism. For example, Bebout *et al*. (1999) demonstrated that the mean boron concentration of metasediments of Catalina Schist, California decrease from 92 ppm for lawsonite-albite facies rocks to 15 ppm for amphibolite-grade equivalents. In Fig. 7, the estimated sediment melt composition (point M) and mantle source (point B) obtained by 3% bulk mixing of melt to depleted mantle are shown. Plots of samples from SSVZ show considerable scattering, although their B/Nb, Ba/Nb, Pb/Nb, and K/Nb ratios are plotted close to the mixing lines of the depleted mantle and estimated sediment melt. The age of subducting plate beneath the SSVZ is young (<10 Ma). Therefore, melting of the cover sediment on the subducting plate is plausible. However, the contribution of slab-derived melt from the mantle source is limited, as inferred from the fact that depletion of heavy REEs is not observed for SSVZ (Fig. 3).

Conclusions

Volcanic rocks of the SVZ generally bear the geochemical signature of arc magmas. Based on the model calculation of trace element composition including boron of the slab-derived fluid, the mantle source of CSVZ volcanic rocks is metasomatized AOC-derived and sediment-derived fluids. In contrast, the mantle source of the SSVZ volcanic rocks with low B/Nb ratios was metasomatized by the melt of sediment that had undergone a loss of boron during subduction zone metamorphism at a shallower level. This contrasting feature might reflect thermal conditions beneath the arc, depending on the age of the subducting oceanic plate.

Acknowledgments—The PGA was conducted at the Inter-University Laboratory for the Joint use of JAEA Facilities. We thank H. Matsue, Y, Sekiya, H. Sawahata, and M. Ishimoto for help in the PGA. The XRF and LA-ICP-MS analyses were supported by the Earthquake Research Institute cooperative research program, The University of Tokyo. We are thankful to N. Hokanishi for help in XRF analysis. M. Tagiri and K. Notsu kindly provided samples obtained from some SSVZ volcanoes (Huequi, Michinmahuida, Corcovad, Melimoyu, Menlolat, and Cay). Many thanks to Prof. Charles R. Stern and an anonymous referee, whose constructive criticism improved the manuscript. This work was partially supported by Grants-in-Aid from the Ministry of Education, Culture, Sports, Science and Technology of Japan (Nos. 17540460 and 21403012) to H.S. and Y.O.

References

Aizawa, Y., Tatsumi, Y. and Yamada, H. (1999) Element transport by dehydration of subducted sediments: Implication for arc and ocean island magmatism. *Island Arc* **8**, 38–46.

Anma, R., Kawamura, K., Orihashi, Y. and Aniya, M. (2009) Sediment core sampling at the Chile triple junction area. In MIRAI Cruise Report MR08-06 Leg 1. JAMSTEC. Available at http://www.godac.jamstec.go.jp/cruisedata/mirai/e/MR08-06_leg1.html

Bebout, G. E. (2007) Metamorphic chemical geodynamics of subduction zones. *Earth Planet. Sci. Lett.* **260**, 373–393.

Bebout, G. E., Ryan, J. G., Leeman, W. P. and Bebout, A. E. (1999) Fractionation of trace elements by subduction-zone metamorphism: Effect of convergent-margin thermal evolution. *Earth Planet. Sci. Lett.* **171**, 63–81.

Behrmann, J. H., Lewis, S. D., Cande, S. and ODP Leg 141 Scientific Party (1994) Tectonics and geology of spreading ridge subduction at the Chile Triple Junction; a synthesis of results from Leg 141 of the Ocean Drilling Program. *Geol. Rund.* **83**, 832–852.

Chaussidon, M. and Marty, B. (1995) Primitive boron isotope composition of the mantle. *Science* **269**, 383–386.

Dixon, H. J., Murphy, M. D., Sparks, S. J., Chavéz, R., Naranjo, J. A., Dunkley, P. N., Young, S. R., Gilbert, J. S. and Pringle, M. R. (1999) The geology of Nevados de Chillán volcano, Chile. *Revista Geológica de Chile* **26**, 227–253.

D'Orazio, M., Innocentia, F., Manetti, P., Tamponia, M., Tonarini, S., González-Ferrán, O., Lahsen, A. and Omarini, R. (2003) The Quaternary calc-alkaline volcanism of the Patagonian Andes close to the Chile triple junction: geochemistry and petrogenesis of volcanic rocks from the Cay and Maca volcanoes (*ca*. 45°S, Chile). *J. South Amer. Earth Sci.* **16**, 219–242.

Futa, K. and Stern, C. R. (1988) Sr and Nd isotopic and trace element compositions of Quaternary volcanic centers of the Southern Andes. *Earth Planet. Sci. Lett.* **88**, 253–262.

Gerlach, D. C., Frey, F. A., Moreno-Roa, H. and López-Escobar, L. (1988) Recent volcanism in the Puyehue-Cordon Caulle region, Southern Andes, Chile (40.5°S): petrogenesis of evolved lavas. *J. Petrol.* **29**, 333–382.

Gonzales-Ferran, O. (1994) *Volcanes de Chile*. Instituto Geografico Militar, Santiago. 640 pp. (in Spanish).

Hervé, F., Faundez, V., Calderon, M., Massonne, H.-J. and Willner, A. P. (2007) Metamorphic and plutonic basement complexes. *The Geology of Chile* (Moreno, T. and Gibbons,

W., eds.), 5–19, Geological Society of London.

Hickey-Vargas, R., Moreno-Roa, H., López-Escobar, L. and Frey, F. A. (1989) Geochemical variations in Andean basaltic and silicic lavas from the Villarrica–Lanin volcanic chain (39.5°S): an evaluation of source heterogeneity, fractional crystallization and crustal assimilation. *Contrib. Mineral. Petrol.* **103**, 361–386.

Hickey-Vargas, R., Sun, M., López-Escobar, L., Moreno-Roa, H., Reagan, M. K., Morris, J. D. and Ryan, J. G. (2002) Multiple subduction components in the mantle wedge: evidence from eruptive centers in the Central Southern volcanic zone, Chile. *Geology* **30**, 199–202.

Hildreth, W. and Moorbath, S. (1988) Crustal contributions to arc magmatism in the Andes of Central Chile. *Contrib. Mineral. Petrol.* **98**, 455–489.

Hoffman, A. W. (1988) Chemical differentiation of the Earth: The relationship between mantle continental crust, and oceanic crust. *Earth Planet. Sci. Lett.* **90**, 297–314.

Ishikawa, T. and Nakamura, E. (1993) Boron isotopic systematics of marine sediments. *Earth Planet. Sci. Lett.* **117**, 567–580.

Ishikawa, T. and Tera, F. (1997) Source, composition and distribution of the fluid in the Kurile mantle wedge: constraints from across-arc variations of B/Nb and B isotopes. *Earth Planet. Sci. Lett.* **152**, 123–138.

Johnson, M. C. and Plank, T. (1999) Dehydration and melting experiments constraint the fate of subducted sediments. *Geochem. Geophys. Geosys.* **1**, 1007, doi:10.1029/1999GC000014.

Kelley, A., Plank, T., Ludden, J. and Staudigel, H. (2003) Composition of altered oceanic crust at ODP Sites 801 and 1149. *Geochem. Geophys. Geosys.* **4**, 8910, doi:10.1029/2002GC000435.

Kilian, R. and Behrmann, J. H. (2003) Geochemical constraints on the sources of Southern Chile Trench sediments and their recycling in arc magmas of the Southern Andes. *J. Geol. Soc. London* **160**, 57–70.

Kogiso, T., Tatsumi, Y. and Nakano, S. (1997) Trace element transport during dehydration processes in the subducted oceanic crust: 1. Experiments and implications for the origin of ocean island basalts. *Earth Planet. Sci. Lett.* **148**, 193–205.

Leeman, W. P. and Sisson, V. B. (1996) Geochemistry of boron and its implications for crustal and mantle processes. *Boron: Mineralogy, Petrology, and Geochemistry* (Grew, E. S. and Anovitz, L. M., eds.), *Rev. Mineral.* **33**, 645–708.

López-Escobar, L., Moreno, H., Tagiri, M., Notsu, K. and Onuma, N. (1985) Geochemistry and petrology of lavas from San José volcano, Southern Andes (33°45′ S). *Geochem. J.* **19**, 209–222.

López-Escobar, L., Parada, M. A., Moreno, H., Frey, F. A. and Hickey-Vargas, R. (1992) A contribution to the petrogenesis of Osorno and Calbuco volcanoes, Southern Andes (41°00′–41°30′ S): comparative study. *Revisita Geológica de Chile* **19**, 211–226.

López-Escobar, L., Kilian, R., Kempton, P. D. and Tagiri, M. (1993) Petrography and geochemistry of Quaternary rocks from the Southern Volcanic Zone of the Andes between 41°30′ and 40°00′, Chile. *Revisita Geológica de Chile* **20**, 33–55.

Lowrie, A. and Hey, R. (1981) Geological and geophysical variations along the western margin of Chile near latitude 33° to 36°S and their relation to Nazca Plate subduction. *Geol. Soc. Amer. Mem.* **154**, 741–754.

Miyoshi, M., Fukuoka, T., Sano, T. and Hasenaka, T. (2008) Subduction influence of Philippine Sea plate on the mantle beneath northern Kyushu, SW Japan: an examination of boron contents in basaltic rocks. *J. Volcanol. Geotherm. Res.* **171**, 73–87.

Moran, A. E., Sisson, V. B. and Leeman, W. P. (1992) Boron depletion during progressive metamorphism: implications for subduction processes. *Earth Planet. Sci. Lett.* **111**, 331–349.

Morris, J. D. and Ryan, J. G. (2003) Subduction zone processes and implications for changing composition of the upper and lower mantle. *Treat. Geochem.* **2**, 451–470.

Morris, J. D., Leeman, W. P. and Tera, F. (1990) The subducted component in island arc lavas: constraints from Be isotopes and B–Be systematics. *Nature* **344**, 31–36.

Naranjo, J. A., Sparks, R. S. J., Stasiuk, M. V., Moreno, H. and Ablay, G. J. (1992) Morphological, structural and textural variations in the 1988–1990 andesite lava of Lonquimay Volcano, Chile. *Geol. Mag.* **129**, 657–678.

Noll, P. D., Jr., Newsom, H. E., Leeman, W. P. and Ryan, J. G. (1996) The role of hydrothermal fluids in the production of subduction zone magmas: Evidence from siderophile and chalcophile trace elements and boron. *Geochim. Cosmochim. Acta* **60**, 587–611.

Orihashi, Y. and Hirata, T. (2003) Rapid quantitative analysis of Y and REE abundances in XRF glass bead for selected GSJ reference rock standards using Nd-YAG 266 nm UV laser ablation ICP-MS. *Geochem. J.* **37**, 401–412.

Orihashi, Y., Naranjo, J. A., Motoki, A., Sumino, H., Hirata, D., Anma, R. and Nagao, K. (2004) Quaternary volcanic activity of Hudson and Lautaro Volcanoes, Chilean Patagonia: new constraints from K–Ar ages. *Revisita Geológica de Chile* **31**, 207–224.

Orihashi, Y., Park, S., Machida, S., Anma, R., Jalowizki, T., de Souza, R., Motoki, A. and Abe, N. (2009) Rock sampling at the subducting ridge segment (Segment 1) In MIRAI Cruise Report MR08-06 Leg 1. JAMSTEC. Available at http://www.godac.jamstec.go.jp/cruisedata/mirai/e/MR08-06_leg1.html

Ottolini, L., Laporte, D., Raffone, N., Devidal, J. and Le Fèvre, B. (2009) New experimental determination of Li and B partition coefficients during upper mantle partial melting. *Contrib. Mineral. Petrol.* **157**, 313–325.

Ramos, V. A. and Kay, S. M. (1992) Southern Patagonian plateau basalts and deformation: backarc testimony of ridge collisions. *Tectonophysics* **205**, 261–282.

Ryan, J. G., Morris, J., Tera, F., Leeman, W. P. and Tsvetkov, A. (1995) Cross-arc geochemical variations in the Kurile Arc as a function of slab depth. *Science* **270**, 625–627.

Sano, T., Fukuoka, T., Hasenaka, T., Yonezawa, C., Matsue, H. and Sawahata, H. (1999) Accurate and efficient determination of boron content in volcanic rocks by neutron induced prompt γ-ray analysis. *J. Radioanal. Nucl. Chem.* **239**, 613–617.

Sano, T., Hasenaka, T., Shimaoka, A., Yonezawa, C. and Fukuoka, T. (2001) Boron contents of Japan Trench sediments and Iwate basaltic lavas, northeast Japan arc: estimation of sediment-derived fluid contribution in mantle wedge. *Earth Planet. Sci. Lett.* **186**, 199–213.

Sigmarsson, O., Condomines, M., Morris, J. D. and Harmon, R. S. (1990) Uranium and ^{10}Be enrichments by fluids in Andean arc magmas. *Nature* **346**, 163–165.

Smith, H. J., Spivack, A. J., Staudigel, H. and Hart, S. R. (1995) The boron isotopic composition of altered oceanic crust. *Chem. Geol.* **126**, 119–135.

Stern, C. R. (2004) Active Andean volcanism: its geologic and tectonic setting. *Revisita Geológica de Chile* **31**, 161–206.

Stern, C. R., Moreno, H., López-Escobar, L., Clavero, J. E., Lara, L. E., Naranjo, J. A., Parada, M. A. and Skewes, M. A. (2007) Chilean Volcanoes. *The Geology of Chile* (Moreno, T. and Gibbons, W., eds.), 147–178, Geological Society of London.

Sun, S.-S. and McDonough, W. F. (1989) Chemical and isotopic systematics of oceanic basalts: implications for mantle composition and processes. *Magmatism in the Ocean Basins* (Saunders, A. D. and Norry, M. J., eds.), *Geol. Soc. Spec. Pub.* **42**, 313–345.

Tani, K., Orihashi, Y. and Nakada, S. (2002) Major and trace components analysis of silicate rocks by X-ray fluorescence spectrometer using fused glass beads: evaluation of analytical precision of three, six, eleven times dilution fused glass beads methods. *Earthquake Research Institute, University of Tokyo Technical Research Report* **8**, 26–36 (in Japanese with English abstract).

Tatsumi, Y. (2000) Continental crust formation by crustal delamination in subduction zones and complementary accumulation of the enriched mantle I component in the mantle. *Geochem. Geophys. Geosys.* **1**, 1053, doi:10.1029/2000GC000094.

Tormey, D. R., Hickey-Vargas, R., Frey, F. A. and López-Escobar, L. (1991) Recent lavas from the Andean front (33° to 42°S): interpretations of along-arc compositional variations. *Geol. Soc. Amer. Spec. Pap.* **265**, 57–77.

Workman, R. K. and Hart, S. R. (2005) Major and trace element composition of the depleted MORB mantle (DMM). *Earth Planet. Sci. Lett.* **231**, 53–72.

Yamazaki, T., Kanamatsu, T., Shimono, T. *et al.* (2009) Paleomagnetism in the southeast Pacific. *MIRAI Cruise Report MR08-06 Leg 1*, JAMSTEC. Available at http://www.godac.jamstec.go.jp/cruisedata/mirai/e/MR08-06_leg1.html

Yonezawa, C. (1993) Prompt γ-ray analysis of elements using cold and thermal reactor guided neutron beams. *Anal. Sci.* **9**, 185–193.

Supplementary Materials

URL (http://www.terrapub.co.jp/journals/GJ/archives/data/47/MS241.pdf)
Table S1